Research Square

Preprints are preliminary reports that have not undergone peer review.
They should not be considered conclusive, used to inform clinical practice,
or referenced by the media as validated information.

Spatially Contrasting Diurnal Rainfall Responses to Cross- Equatorial Northerly Surges Over the Southwestern Maritime Continent and Their Modulation by Mjo Phase and Enso State

Muhamad Djazim Syaifullah

muha042@brin.go.id

National Research and Innovation Agency

Ardhi Adhary Arbain

National Research and Innovation Agency

Rahmawati Syahdiza

National Research and Innovation Agency

Findy Renggono

National Research and Innovation Agency

Cornelius Antoni Nababan

National Research and Innovation Agency

Purwadi Purwadi

National Research and Innovation Agency

Research Article

Keywords: Cross-Equatorial Northerly Surge, Madden-Julian Oscillation, Diurnal Rainfall Cycle, Maritime Continent, Boreal Winter

Posted Date: November 12th, 2026

DOI: https://doi.org/10.21203/rs.3.rs-10798240/v1

License: This work is licensed under a Creative Commons Attribution 4.0 International License.
Read Full License

Additional Declarations: No competing interests reported.

SPATIALLY CONTRASTING DIURNAL RAINFALL RESPONSES TO CROSS-EQUATORIAL NORTHERLY SURGES OVER THE SOUTHWESTERN MARITIME CONTINENT AND THEIR MODULATION BY MJO PHASE AND ENSO STATE

Author :
Muhamad Djazim Syaifullah[1*][0009-0005-8265-2620], Ardhi Adhary Arbain[1][0000-0002-2347-7974], Rahmawati Syahdiza[1][0000-0002-4970-4362], Findy Renggono[1][0000-0001-6758-0247], Cornelius Antoni Nababan [2][0009-0008-0120-6840] and Purwadi [1][0000-0002-2926-7302].

[1]Research Center for Climate and Atmosphere, National Research and Innovation Agency, Serpong 15314, Indonesia
[2]Directorate for Laboratory Management, Research Facilities, and Science and Technology Park, National Research and Innovation Agency, Serpong 15314, Indonesia

* Corresponding address: muha042@brin.go.id

Abstract

Cross-equatorial northerly surges (CENS) drive extreme rainfall and flooding over the southwestern Maritime Continent during boreal winter, but the physical mechanisms linking CENS to large-scale climate variability and the diurnal rainfall cycle remain incompletely understood. Using ERA5 reanalysis, GSMaP hourly satellite precipitation, and the Real-time Multivariate MJO index over 25 boreal winters (DJF 2001–2025), this study investigates CENS characteristics, their modulation by the MJO, ENSO, and IOD, and their spatially contrasting effects on the diurnal rainfall cycle across an ocean-to-land gradient. A total of 52 CENS events were identified (2.08 events per year). La Niña conditions account for 53.8% of events and enhance CENS frequency partly through prolonged active MJO conditions rather than solely through direct monsoon strengthening. A statistically significant association between ENSO state and MJO phase distribution is confirmed ($\chi^2 = 33.779$, $p = 0.0022$). While CENS event-days are most frequent during MJO phases 6–7, the most intense rainfall occurs during phases 4–5. This paradox is explained by phase-dependent differences in boundary-layer moisture-convergence efficiency, supported by 925 hPa moisture-flux diagnostics. Lagged correlation analysis, filtered for Maritime Continent-active MJO phases, shows that MJO activity precedes CENS intensification by 3–6 days ($r = -0.074$, $p < 0.001$). Most critically, CENS suppresses oceanic rainfall by 70–80% throughout the diurnal cycle while simultaneously amplifying nocturnal land rainfall by approximately a factor of two, with statistically significant peaks at 02:00–04:00 LT. This spatially contrasting diurnal reorganization—first documented here through a systematic CENS versus non-CENS day comparison—has implications for flood-risk management and multi-scale early warning systems for western Java.

Keywords : Cross-Equatorial Northerly Surge; Madden-Julian Oscillation; Diurnal Rainfall Cycle; Maritime Continent; Boreal Winter

1. INTRODUCTION

The Maritime Continent (MC) — encompassing the Indonesian archipelago, the Philippines, and surrounding seas — sits astride the equator and receives abundant solar radiation throughout the year, sustaining high sea surface temperatures, persistent moisture availability, and intense convective activity. These conditions make rainfall variability over the MC one of the most consequential climate signals in the tropics, shaping regional monsoon patterns and driving extreme weather events (Aldrian and Susanto 2003; Chang et al. 2005). Rainfall distribution across the region is highly heterogeneous: Sumatra, Borneo, and Papua receive consistently high annual rainfall, while Java, Bali, and parts of Sulawesi experience a pronounced monsoonal cycle with a wet season from November to March and a dry season from April to October. In densely populated lowland areas such as Jakarta, heavy rainfall events frequently trigger devastating floods, exacerbated by rapid urbanization and inadequate drainage infrastructure. Major flood events in 2007, 2013, and 2020 each resulted in extensive property damage, population displacement, and casualties (Wu et al. 2007; Wu et al. 2013; Budiyono et al. 2015; Lubis et al. 2022). One of the principal synoptic-scale systems responsible for triggering these events is the cold surge (CS) — a rapid equatorward penetration of cold, dry air from continental high-pressure systems over the Northern Hemisphere, typically persisting for several days and characterized by enhanced surface winds and abrupt temperature drops (Chang et al. 2005). The frequency and intensity of CS events are modulated by large-scale circulation patterns (Xavier et al. 2020) and interannual climate variability (Heo et al. 2018).

A related but distinct phenomenon is the Cross-Equatorial Northerly Surge (CENS) — a sustained, low-level northerly flow originating from Asian high-pressure systems that transports cold and dry air across the equator into the southern MC (Hattori et al. 2011). CENS events occur episodically during boreal winter, typically lasting from several days to

approximately one week, with considerable variability in intensity and spatial extent. While CENS can develop in association with CS events — with the cold surge providing the initial northerly momentum that subsequently crosses the equator — a substantial fraction of CENS events are driven by tropical processes, including the Madden–Julian Oscillation (MJO) and equatorial waves, without a clear extratropical precursor (Hattori et al. 2011; Moteki 2024; Hadi et al. 2025). Over the southwestern MC, the interaction between CENS and CS strengthens low-level northerly flow and enhances cross-equatorial moisture transport, intensifying convection and generating heavy rainfall along the northern coast of Java (Chang et al. 2005; Wu et al. 2007; Hattori et al. 2011; Yulihastin et al. 2020; Maulana et al. 2023; Satiadi et al. 2023; Lubis et al. 2023; Hadi et al. 2025). The role of CENS in modifying the timing and amplitude of diurnal rainfall cycles has been documented in multiple observational studies, with nocturnal rainfall over coastal and inland areas of western Java showing marked intensification during active CENS periods (Wu et al. 2007; Trilaksono et al. 2012; Yulihastin et al. 2020; Lubis et al. 2023).

The foundational work of Hattori et al. (2011) established a classification framework for CENS events based on their associated weather patterns, demonstrating that enhanced northerly flow between October and April is systematically linked to increased rainfall along the northern coast of Java. Subsequent studies have progressively revealed the multi-scale nature of CENS forcing. Xavier et al. (2020) showed that CS activity over Southeast Asia varies seasonally and that the MJO can either amplify or suppress CENS development depending on its phase, highlighting the importance of intraseasonal variability as a modulating factor. Trismidianto et al. (2023) further examined the three-way interaction among CS, CENS, and the Borneo Vortex (BV), showing how MJO phase modulates the combined rainfall response during the wet season. The dominant role of CS in controlling BV occurrence was subsequently confirmed by Crook et al. (2024). Taken together, these findings establish that CENS dynamics are governed by forcings operating across multiple scales: synoptic-scale systems such as CS and the BV, and planetary-scale intraseasonal variability represented by the MJO.

The spatial heterogeneity of CENS impacts across the southwestern MC has been increasingly recognized in recent work. Maulana et al. (2023) documented the longitudinal variation of CENS influence across Java, showing that the strongest response occurs in western Java and diminishes progressively eastward. Complementing this, Satiadi et al. (2023) examined the latitudinal structure of CENS effects across five sub-regions of West Java — from mountainous inland areas to offshore waters — finding that coastal areas experience the largest rainfall enhancement, reaching approximately 215% above climatological values during active CENS periods. Both studies concur that CENS promotes morning rainfall enhancement over coastal and offshore areas while suppressing afternoon convection inland. However, a critical gap remains: no study has systematically quantified how CENS modifies the diurnal rainfall cycle across the full ocean-to-land gradient, nor has the CENS-induced diurnal anomaly been explicitly isolated from the background climatological signal by comparing CENS days directly against non-CENS days within the same season. This distinction is essential for attributing observed diurnal changes to CENS forcing rather than to other co-occurring factors such as land-sea breeze dynamics or large-scale monsoonal flow.

At the large-scale, CENS events have been shown to reinforce the southward detour of the MJO across the MC during boreal winter by strengthening northwesterly and westerly winds and enhancing zonal moisture convergence (Lubis et al. 2023). Moteki (2024) demonstrated that CENS events intensify preferentially during La Niña conditions and active MJO phases, while Hadi et al. (2025) showed that 41% of CENS occurrences develop without a cold surge precursor, driven instead by tropical intraseasonal processes including MJO phases 4–7, Mixed-Rossby-Gravity waves, Equatorial Rossby waves, and tropical cyclones — events that nonetheless produce rainfall anomalies and flood risks comparable to their CS-triggered counterparts. Despite these advances, three critical questions remain unresolved. First, whether the influence of the MJO on CENS operates independently across its phases or is partially mediated through ENSO-driven changes in MJO behavior has not been formally tested. Second, while the dynamical mechanism linking MJO convective forcing to northerly flow intensification has been inferred from composite analyses, direct temporal evidence for MJO activity preceding CENS development — particularly when MJO convection is active over the MC itself — remains lacking. Third, and most critically, no study has systematically characterized how CENS reorganizes the diurnal rainfall cycle across the ocean-to-land gradient of the southwestern MC, nor has the CENS-induced diurnal signal been isolated from the background climatological cycle through a direct CENS versus non-CENS day comparison.

To address these gaps, this study investigates the characteristics and large-scale modulation of CENS events over the southwestern MC (0°–7.5°S, 105°E–110°E) during boreal winter (December–February) over a 25-year period from 2001 to 2025, using ERA5 reanalysis winds, GSMaP hourly satellite precipitation, and the Real-time Multivariate MJO index. CENS events are identified following the original area of Hattori et al. (2011) to ensure methodological consistency with prior literature. Three specific objectives are addressed: (1) to quantify the temporal characteristics and large-scale climate modulation of CENS events, including the roles of the MJO, ENSO, and the Indian Ocean Dipole (IOD) as a secondary co-modulator; (2) to provide dynamical evidence for the MJO–CENS relationship

through lagged correlation analysis filtered for Maritime Continent-active MJO phases, supported by 925 hPa moisture flux diagnostics; and (3) to characterize the spatially contrasting diurnal rainfall responses to CENS across oceanic, coastal, and land areas through a systematic CENS versus non-CENS day comparison. The remainder of the paper is organized as follows: Section 2 describes the data and methods; Section 3 presents the results; Section 4 discusses the findings in the context of existing literature; and Section 5 provides the conclusions.

2. MATERIALS AND METHODS

2.1. Study Area

This study focuses on the region spanning 0°–7.5°S, 105°E–110°E, encompassing the Karimata Strait, the western Java Sea, the northern coast of western Java Island, and parts of Lampung Province, Indonesia (Figure 1). To characterize the spatially contrasting diurnal rainfall responses to CENS across the ocean-to-land gradient — one of the primary objectives of this study — the area is subdivided into three sub-areas based on their dominant surface type and proximity to the coastline. Area 1 (black box, 0°–2.5°S, 105°E–110°E) is predominantly oceanic, bordering the equator, and represents the region of initial CENS impact where northerly flow first interacts with the warm sea surface. Area 2 (red box, 2.5°S–5.0°S, 105°E–110°E) covers the transition zone between the open ocean and the coastline, capturing the mixed ocean-coastal response to northerly surges. Area 3 (blue box, 5.0°S–7.5°S, 105°E–110°E) encompasses the eastern coastal zone of Lampung Province and the northern lowlands of western Java — a region of high population density and documented vulnerability to CENS-driven extreme rainfall and flooding. The three-area framework thus provides a systematic cross-section through which the CENS-induced modification of the diurnal cycle can be evaluated from the open ocean to the land interior.

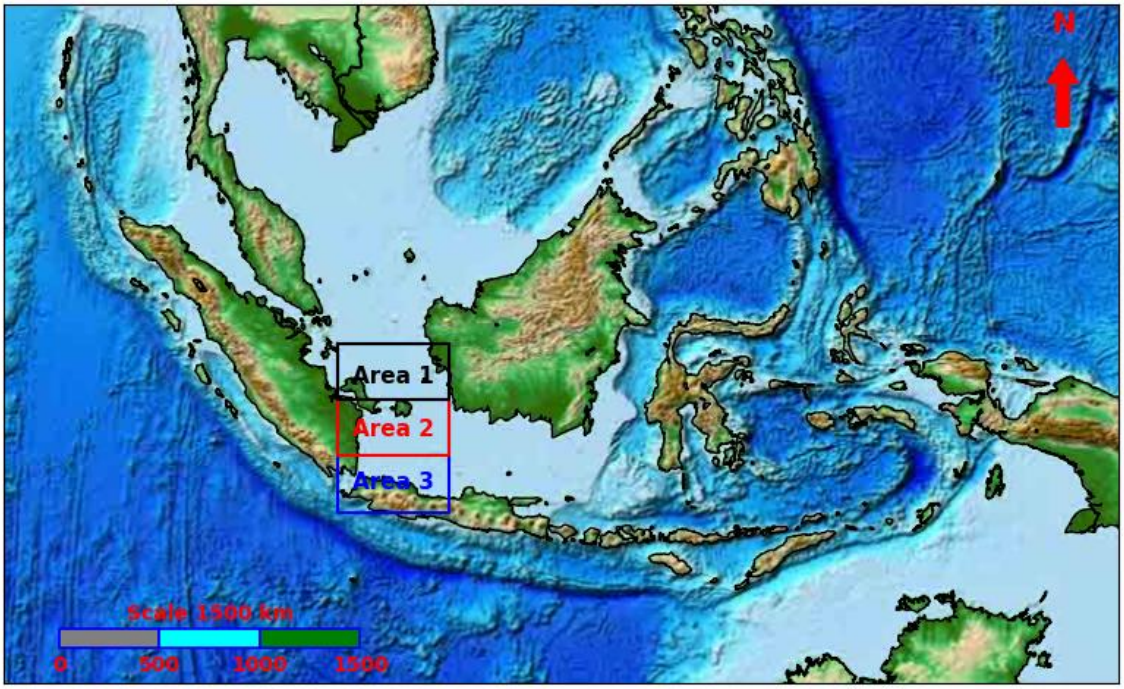


Figure 1. Study Area

It is acknowledged that the study area (0°–7.5°S, 105°E–110°E) constitutes a subregion of the broader Maritime Continent, with findings most directly applicable to the Karimata Strait, Jakarta Bay, and the northern coast of western Java. Generalizations to the wider MC should therefore be made with appropriate caution, recognizing that CENS impacts exhibit substantial spatial heterogeneity across the archipelago (Maulana et al. 2023; Satiadi et al. 2023).

2.2. Data

CENS and CS events were identified using ERA5 (ECMWF Reanalysis v5), a global atmospheric reanalysis produced by the European Centre for Medium-Range Weather Forecasts (ECMWF) with a horizontal resolution of approximately 0.25° × 0.25° (~27 km) and available from 1940 to the present (Hersbach et al. 2020; Hersbach et al. 2023). Hourly meridional and zonal wind components at the 925 hPa pressure level were extracted for the period

2001–2025 to identify CENS events and compute the CENS index. Additionally, ERA5 specific humidity at 925 hPa was extracted over the broader area (15°N–15°S, 90°E–130°E) to compute 925 hPa moisture flux and moisture flux divergence composites, providing dynamical evidence for the MJO–CENS relationship across different MJO phase groups.

The MJO was characterized using the Real-time Multivariate MJO (RMM) index provided by the Australian Bureau of Meteorology (BoM), which is available as daily data from 1974 to the present (Wheeler and Hendon 2004; Straub 2013; Liu et al. 2016). The RMM index consists of two principal components (RMM1 and RMM2) derived from combined fields of outgoing longwave radiation and 850 and 200 hPa zonal winds, with the MJO phase and amplitude computed as the angular position and magnitude of the RMM1–RMM2 vector.

ENSO conditions were represented by the Niño 3.4 index, defined as monthly sea surface temperature (SST) anomalies averaged over 5°N–5°S, 170°W–120°W relative to the 1981–2010 climatology, obtained from the NOAA Physical Sciences Laboratory (Rayner et al. 2003). The Niño 3.4 index is widely used as the primary ENSO monitoring index due to its ability to capture basin-scale SST variability (Barnston et al. 1997). El Niño and La Niña events were identified using the NOAA Oceanic Niño Index (ONI), defined as a Niño 3.4 anomaly exceeding ±0.5°C sustained over five consecutive overlapping three-month seasons.

To examine the potential secondary role of the Indian Ocean Dipole (IOD) as a co-modulator of CENS activity, the Dipole Mode Index (DMI) was obtained from NOAA-PSL. The DMI is defined as the SST anomaly difference between the western (50°E–70°E, 10°N–10°S) and eastern (90°E–110°E, 10°S–0°) tropical Indian Ocean boxes (Saji et al. 1999). IOD states were classified using the preceding September–November (SON) mean DMI, with positive (DMI > +0.4°C) and negative (DMI < −0.4°C) events identified following standard conventions.

Rainfall variability was analyzed using the Global Satellite Mapping of Precipitation Near-Real-Time gauge-adjusted product (GSMaP_GNRT version 6), produced by the Japan Aerospace Exploration Agency (JAXA) as part of the Global Precipitation Measurement (GPM) mission. This product is distributed with a spatial resolution of 0.1° × 0.1° (~11 km) and an hourly temporal resolution, processed approximately four hours after observation. The gauge-adjusted product demonstrates higher accuracy than uncorrected retrievals, particularly over land areas (Kubota et al. 2020). Hourly GSMaP data covering the period 2001–2025 were used to construct diurnal rainfall composites for CENS and non-CENS days across the three study areas.

2.3. Methods

CENS events were identified following Hattori et al. (2011) as periods during which the daily mean 925 hPa northerly wind, area-averaged over 0°–5°S, 105°E–115°E, equaled or exceeded 5 m s^{-1} for at least three consecutive days. Each qualifying period was treated as a single CENS event. While Hattori et al. (2011) originally employed QuikSCAT sea surface winds, the use of ERA5 925 hPa reanalysis over this predominantly oceanic area is consistent with subsequent studies applying the same definition (Moteki 2024; Lubis et al. 2022, 2023; Satiadi et al. 2023). CS events were identified following Chang et al. (2005) as periods when the daily mean meridional wind at 15°N within 110°E–117.5°E fell below −8 m s^{-1} for at least two consecutive days. Daily means were derived from ERA5 hourly wind data.

The RMM amplitude was computed as $\sqrt{(RMM1^2 + RMM2^2)}$. Active MJO conditions were defined as RMM amplitude ≥ 1.0 during December–February (DJF). Following Wheeler and Hendon (2004), MJO phases 2–3 indicate enhanced convection over the Indian Ocean, phases 4–5 over the Maritime Continent, phases 6–7 over the Western Pacific, and phases 8–1 over the Western Hemisphere and Africa. For the purpose of lagged correlation analysis, Maritime Continent-active MJO conditions were defined as days with RMM amplitude ≥ 1.0 and phase within 3–7, following the reviewer recommendation of Reviewer 1 to gate the analysis on phases physically relevant to CENS forcing.

El Niño and La Niña events were defined using the NOAA Oceanic Niño Index (ONI), with Niño 3.4 anomalies exceeding ±0.5°C sustained over five consecutive overlapping three-month seasons (Barnston et al. 1997; Trenberth 1997). To examine the potential secondary modulating role of the Indian Ocean Dipole (IOD), CENS events were classified according to the preceding SON-mean DMI, with IOD-positive (DMI > +0.4°C), IOD-negative (DMI < −0.4°C), and neutral conditions identified following Saji et al. (1999).

To examine the temporal relationship between MJO activity and CENS development, Pearson lagged correlations were computed between daily RMM amplitude and the area-averaged 925 hPa meridional wind over the study area (0°–7.5°S, 105°E–110°E) for lags of ±15 days. Two complementary analyses were performed: (a) using all DJF days to provide a general overview of the MJO–CENS temporal relationship, and (b) restricted to days with active MJO convection over the Maritime Continent (RMM ≥ 1.0, phases 3–7) to isolate the physical link between MJO convective forcing and northerly flow intensification. Statistical significance was assessed using two-tailed Pearson correlation tests, and 95% confidence intervals were estimated through bootstrap resampling (n = 1000 iterations).

To provide dynamical evidence for MJO modulation of CENS, composite anomalies of 925 hPa moisture flux and moisture flux divergence (MFD) were computed for CENS days relative to non-CENS DJF days, stratified by MJO phase group. The zonal and meridional moisture flux components were calculated as MF_u = q × u and MF_v = q × v, where q is the ERA5 925 hPa specific humidity and u, v are the zonal and meridional wind components, respectively. The MFD was computed as the horizontal divergence of the moisture flux vector: MFD = ∂(MF_u)/∂x + ∂(MF_v)/∂y, where negative values indicate moisture convergence. Composites were computed over the broader area (15°N–15°S, 90°E–130°E) to capture the large-scale moisture transport patterns associated with CENS under different MJO phase conditions.

To isolate the contribution of CENS to the diurnal rainfall cycle from background climatological effects — such as land-sea breeze dynamics and orographic forcing — composite mean hourly rainfall was computed separately for CENS days and non-CENS DJF days across the three study areas, using GSMaP hourly data for the period 2001–2025. All times are expressed in local time (LT; UTC+7). The statistical significance of the difference between CENS and non-CENS diurnal composites at each hour was assessed using a two-sample Welch's t-test ($p < 0.05$). This CENS versus non-CENS framework enables a direct attribution of diurnal anomalies to CENS forcing, distinguishing the CENS signal from the background seasonal diurnal cycle.

Time–longitude Hovmöller diagrams of daily meridional wind and GSMaP precipitation were constructed for each DJF season over the study period to visualize the temporal evolution and spatial propagation of individual CENS events and their associated rainfall responses.

3. RESULTS

3.1. CENS Event Characteristics during DJF 2001–2025

A total of 52 CENS events were identified during December–February (DJF) over the 25-year period from 2001 to 2025, corresponding to a mean occurrence rate of 2.08 events per year. This frequency is lower than the 2.85 events per year reported by Hadi et al. (2025) and substantially lower than the 6.2 events per year reported by Hattori et al. (2011). The differences are primarily attributable to variations in the CENS identification methodology, including the analysis period, identification area, and threshold definition. Hadi et al. (2025) applied the standard deviation-based index of Maulana et al. (2023) over a narrower area (105°–110°E), whereas the present study adopts the absolute wind-speed threshold of Hattori et al. (2011) over the wider 105°–115°E area. Hattori et al. (2011) further used QuikSCAT sea-surface winds and included DJFM, whereas the present analysis is restricted to DJF using ERA5 data. Thus, the differences in occurrence rates should be interpreted primarily as methodological rather than physical discrepancies, and the value obtained in this study remains within the range reported for CENS across different datasets and identification criteria.

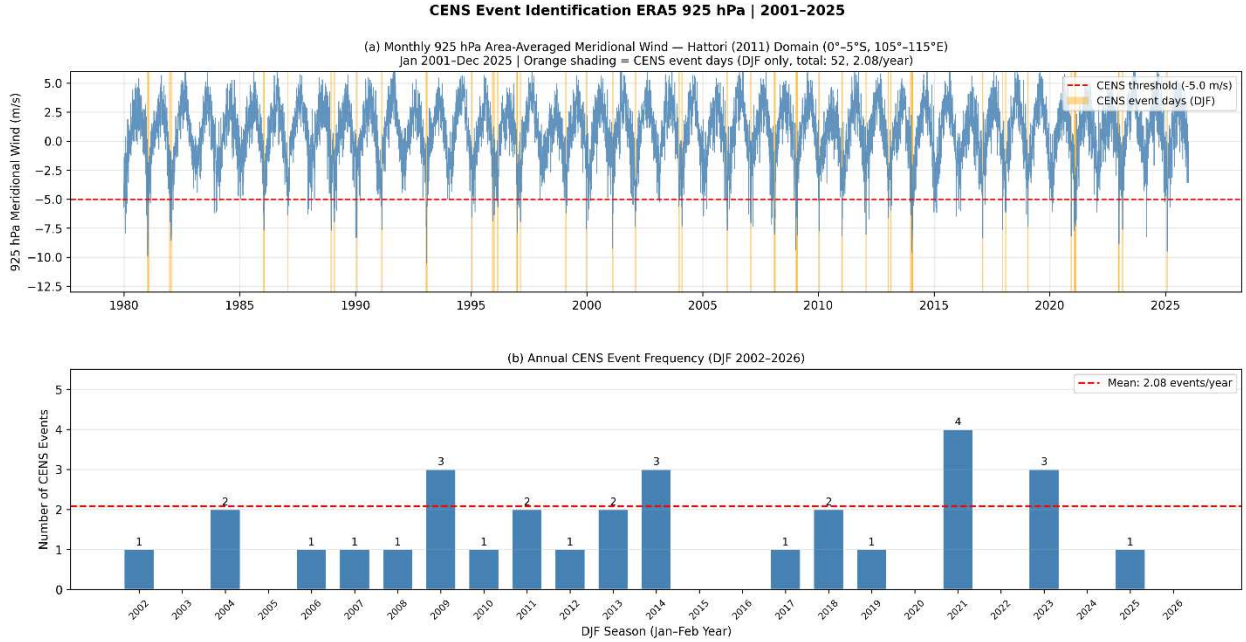


Figure 2. CENS event identification

The total number of CENS event-days over the study period was 276, accounting for approximately 6.65% of all DJF days. CENS events occurred in 17 of the 25 DJF seasons examined, with notable inter-annual variability (Figure 2b). The highest annual frequency was observed during DJF 2020/2021, with four events recorded, followed by DJF 2008/2009, 2013/2014, and 2022/2023, each recording three events. No CENS events were identified during DJF 2002/2003, 2004/2005, 2009/2010, 2014/2015, 2015/2016, 2019/2020, 2021/2022, and 2023/2024. The clustering of active years around known La Niña periods — particularly 2010/2011, 2020/2021, and 2022/2023 — is consistent with the enhanced northerly monsoon flow associated with La Niña conditions, as documented by Moteki (2024) and Hadi et al. (2025).

Table 1. Duration Distribution of CENS

Duration	Count	Percentage	Duration	Count	Percentage
3	18	34.6%	8	2	3.8%
4	8	15.4%	9	1	1.9%
5	7	13.5%	10	2	3.8%
6	6	11.5%	16	2	3.8%
7	6	11.5%			

The distribution of CENS event durations is summarized in Table 1. Event durations ranged from 3 to 16 days, with the majority of events (45 events, 87%) lasting between 3 and 7 days, consistent with the synoptic timescale of cold surge forcing over the Maritime Continent. Events lasting 8–10 days accounted for 5 events (10%), while only 2 events (4%) exceeded 10 days. The predominance of short-duration events suggests that sustained CENS development beyond one week requires a combination of persistent large-scale forcing — such as prolonged La Niña conditions or an MJO active phase co-located over the Maritime Continent — rather than episodic cold surge intrusions alone. CENS events were most frequently initiated in January, followed by December and February, reflecting the peak of the Asian winter monsoon circulation during these months.

Table 2. MJO phase frequency (RMM ≥ 1.0 per phase)

MJO Phase	Phase8	Phase7	Phase6	Phase5	Phase4	Phase3	Phase2	Phase1	Neutral
Event CENS	1	9	18	6	6	0	0	0	12

The distribution of active MJO days (RMM amplitude ≥ 1.0) across the eight RMM phases during DJF 2001–2025 is presented in Table 2. Phases 6 and 7, corresponding to MJO convection over the Western Pacific, recorded the highest frequencies, followed by phases 4–5. Phases 1, 2, 3 and 8 were least frequent. This phase preference reflects the well-documented eastward propagation of the MJO from the Indian Ocean through the Maritime Continent during boreal winter (Wheeler and Hendon 2004), with the MJO residing longest in the Western Pacific phases during DJF.

3.2. Large-Scale Climate Modulation of CENS

3.2.1. Association with MJO, ENSO, and Cold Surge

The distribution of the 52 identified CENS events across combinations of MJO activity, ENSO state, and cold surge (CS) co-occurrence is summarized in Table 3. Of the 52 events, 40 (76.9%) occurred during active MJO conditions (RMM amplitude ≥ 1.0), while 12 events (23.1%) developed during MJO-neutral periods, indicating that active MJO convection is a frequent but not necessary precondition for CENS development. In terms of ENSO state, CENS events were most prevalent during La Niña (28 events, 53.8%), followed by neutral conditions (19 events, 36.5%), with only 5 events (9.6%) occurring during El Niño. The elevated CENS frequency during La Niña is consistent with enhanced Asian winter monsoon flow and stronger northerly low-level winds under cold ENSO conditions, as documented by Moteki (2024) and Hadi et al. (2025).

Table 3. Cross-tabulation CENS, MJO, ENSO, CS

ENSO	MJO+CS	MJO+noCS	noMJO+CS	noMJO+noCS	Total
La Nina	18	6	2	2	28

Neutral	11	3	3	2	19
El-Nino	1	1	3	0	5
Total	30	10	8	4	52

Regarding CS co-occurrence, 38 events (73.1%) developed in association with a CS, while 14 events (26.9%) occurred without a detectable CS — consistent with the CENS-noCS category identified by Hadi et al. (2025), who reported that approximately 41% of CENS events over a longer 42-year record were driven by tropical processes without extratropical precursors. The combined forcing most frequently observed was MJO active + CS, accounting for 30 events (57.7%), with La Niña years contributing the largest subset (18 events). In contrast, the combination of MJO-neutral + no CS was least common (4 events, 7.7%), underscoring the importance of at least one large-scale forcing mechanism — either an active MJO or a cold surge — for CENS initiation. A notable limitation is the small sample sizes in several sub-categories, particularly El Niño (5 events total), which precludes robust statistical inference for those subsets and warrants cautious interpretation.

3.2.2. ENSO–MJO Phase Interaction

To examine whether ENSO modulates CENS activity independently or primarily through its influence on MJO behavior, the distribution of active MJO phase-days (RMM ≥ 1.0) across ENSO states was analyzed for DJF 2001–2025, comprising a total of 1,609 active MJO days (Table 4). A chi-square test reveals a statistically significant association between ENSO state and MJO phase distribution ($\chi^2 = 33.779$, df = 14, $p = 0.0022$), indicating that the preferred MJO phase during boreal winter differs systematically across ENSO conditions.

Table 4. MJO Phase Distribution (Active MJO days, RMM ≥ 1.0)

Enso State / Phase	1	2	3	4	5	6	7	8	Total
El-Nino	28	41	66	78	81	100	110	54	558
La-Nina	22	64	95	68	90	112	145	47	643
Neutral	39	38	40	45	68	65	79	34	408
Total	89	143	201	191	239	277	334	135	1609

Table 5. Percentage (%) per ENSO state

Enso State / Phase	1	2	3	4	5	6	7	8
El-Nino	5.0	7.3	11.8	14.0	14.5	17.9	19.7	9.7
La-Nina	3.4	10.0	14.8	10.6	14.0	17.4	22.6	7.3
Neutral	9.6	9.3	9.8	11.0	16.7	15.9	19.4	8.3

La Niña seasons were associated with the highest number of active MJO days (643 days), compared to El Niño (558 days) and neutral ENSO (408 days), suggesting that La Niña prolongs the duration of active MJO convection during DJF. The phase percentage distributions reveal important differences across ENSO states: during La Niña, MJO phases 6–7 (Western Pacific convection) were most prominent, accounting for 40.0% of active days, compared to 37.6% during El Niño and 35.3% during neutral conditions. Conversely, neutral ENSO seasons showed a relatively more uniform phase distribution, with a slightly higher contribution from phases 1 and 2 (early Indian Ocean phases) compared to La Niña and El Niño. These results suggest that while ENSO significantly modulates the frequency and

phase preference of active MJO conditions, the dominance of phases 6–7 is a robust feature across all ENSO states — consistent with the known eastward propagation preference of the boreal winter MJO. Given that CENS event-days are most frequent during MJO phases 6–7 (Table 5), these findings collectively suggest that La Niña enhances CENS frequency partly by increasing the total duration of MJO-active conditions, particularly in the phases most conducive to northerly flow development over the southwestern MC.

3.2.3. IOD as a Secondary Co-modulator

The potential role of the Indian Ocean Dipole (IOD) as a secondary modulator of CENS activity was examined by classifying CENS events according to the preceding SON-mean DMI (Figure 3). Of the 52 events, the large majority (36 events, 69.2%) occurred during neutral IOD conditions ($|DMI| \leq 0.4°C$), while 13 events (25.0%) developed during IOD-negative periods and only 3 events (5.8%) during IOD-positive conditions (Figure 3a). The cross-classification with ENSO state (Figure 3b) reveals that the predominance of neutral IOD is consistent across La Niña (20 neutral, 5 negative, 0 positive from La Niña subset visible in Figure), neutral ENSO (14 neutral, 8 negative, 2 El Niño), and El Niño (3 positive) conditions.

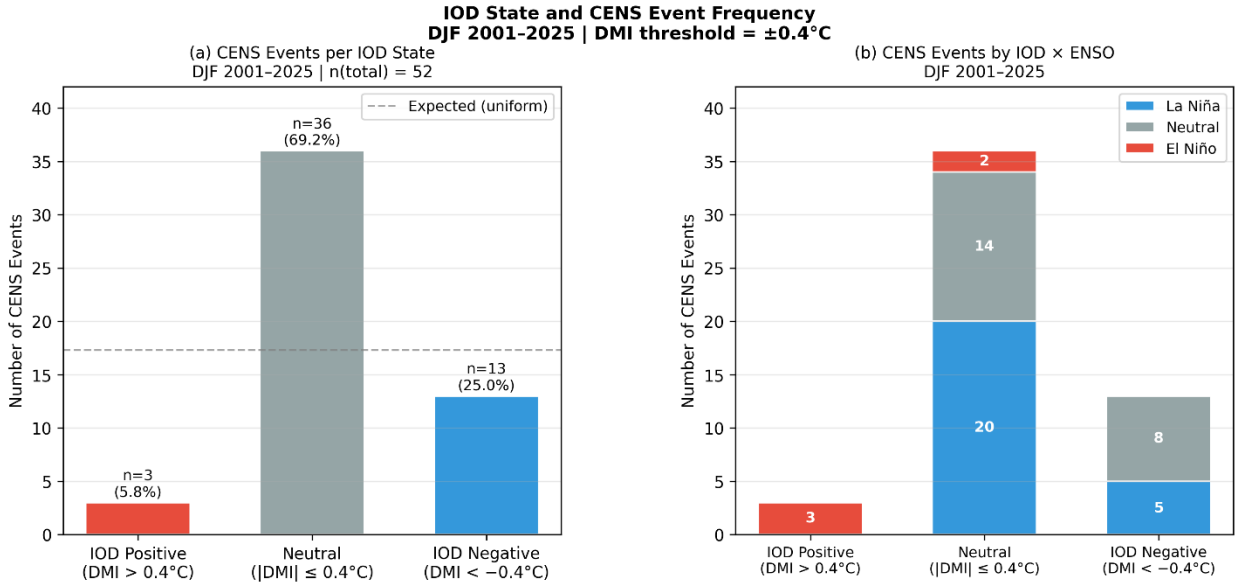


Figure 3. IOD State and CENS Event Frequency

The marginally higher frequency of CENS events during IOD-negative compared to IOD-positive conditions is physically plausible: IOD-negative years are associated with anomalous warming in the eastern tropical Indian Ocean and suppressed convection over the western Indian Ocean, which may enhance cross-equatorial pressure gradients favorable for northerly flow development. However, given the small sample sizes — particularly for IOD-positive events (n = 3) — robust statistical conclusions cannot be drawn. The IOD is therefore treated as a secondary co-modulator in this study, with its influence on CENS likely operating indirectly through its modulation of the background SST gradient and associated changes in monsoon circulation, rather than through a direct dynamical mechanism. Future studies with longer observational records will be needed to more definitively characterize the IOD–CENS relationship.

3.3. Dynamical Evidence for MJO–CENS Relationship

3.3.1. Lagged Correlation between MJO Activity and CENS

The temporal relationship between MJO activity and CENS development was examined through lagged Pearson correlation between daily RMM amplitude and the area-averaged 925 hPa CENS index over the study area (Figure 4). For all DJF days (Figure 4a), the correlation becomes statistically significant beginning at lag −6 days and peaks at lag −1 day ($r = -0.047$, $p < 0.05$), with a broad window of significant negative correlations spanning lag −6 to +10 days. The negative sign indicates that higher RMM amplitude is associated with stronger northerly flow, consistent with MJO-enhanced CENS conditions. When the analysis is restricted to days with active MJO convection over the Maritime Continent (phases 3–7, RMM ≥ 1.0; Figure 4b), the lagged correlation strengthens notably (peak $r = -0.074$, $p < 0.001$), with the significant window becoming more coherent (lag −3 to +13 days). The strengthening of the correlation under MC-active MJO conditions — compared to the phase-blind all-DJF analysis — confirms that the

MJO amplitude–CENS relationship reflects a genuine physical modulation of northerly flow by MJO convective forcing when the MJO is positioned over the Maritime Continent, rather than a statistical artifact driven by high-amplitude MJO events in non-MC phases. The quasi-simultaneous nature of the peak correlation (lag ≈ −1 to +2 days) is consistent with the rapid low-level circulation response to MJO convective heating documented by Lubis et al. (2023) for cross-equatorial surge dynamics over the southwestern Maritime Continent.

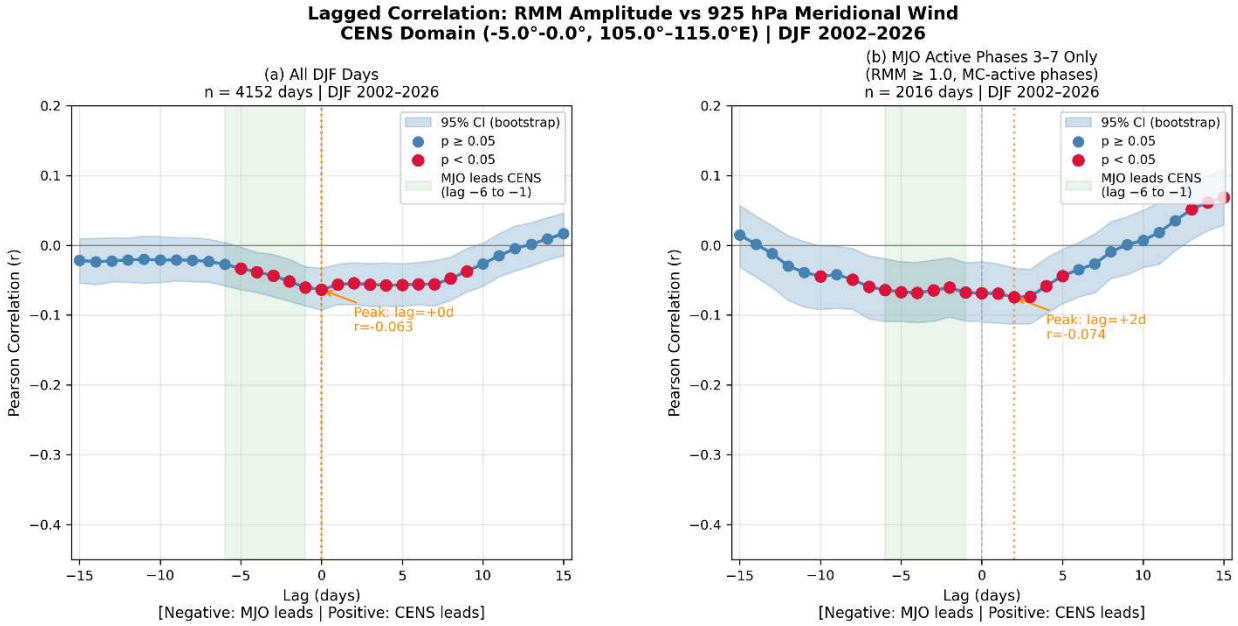


Figure 4. Lagged Correlation between MJO Activity and CENS

3.3.2. Moisture Moisture Flux Composite per MJO Phase group

To provide spatial dynamical evidence complementing the lagged correlation analysis, composite 925 hPa moisture flux and moisture flux divergence (MFD) were computed for CENS days, stratified by MJO phase group (Figure 5 — absolute composite), and compared against non-CENS DJF days to isolate the CENS-specific anomaly signal (Figure 6 — anomaly composite).

The absolute moisture flux composites during CENS days (Figure 5) reveal a consistent large-scale northerly flow pattern across all MJO phase groups, with strong cross-equatorial transport from the South China Sea into the southwestern MC. During MJO phases 3–5 — when MJO convection is active over the Maritime Continent (n = 48 CENS days) — the northerly moisture flux is most organized and the MFD over the study area (0°–7.5°S, 105°–110°E) shows the strongest convergence signal, indicating efficient channeling of moisture from the South China Sea toward the northern coast of Java. During MJO phases 6–7 (n = 84 CENS days), the northerly flow remains strong — consistent with the highest CENS event-day frequency observed in this phase group — but the MFD convergence over the study area is comparatively weaker, reflecting the displacement of the main MJO convective envelope to the Western Pacific and reduced direct convective forcing over the MC. During MJO-neutral conditions (n = 27 CENS days), the moisture flux pattern is less organized, with weaker northerly flow and a more fragmented MFD structure over the study area. The MJO phases 1–2 composite (n = 2 CENS days) is based on an insufficient sample size and is presented for completeness only; no physical interpretation is drawn from this panel.

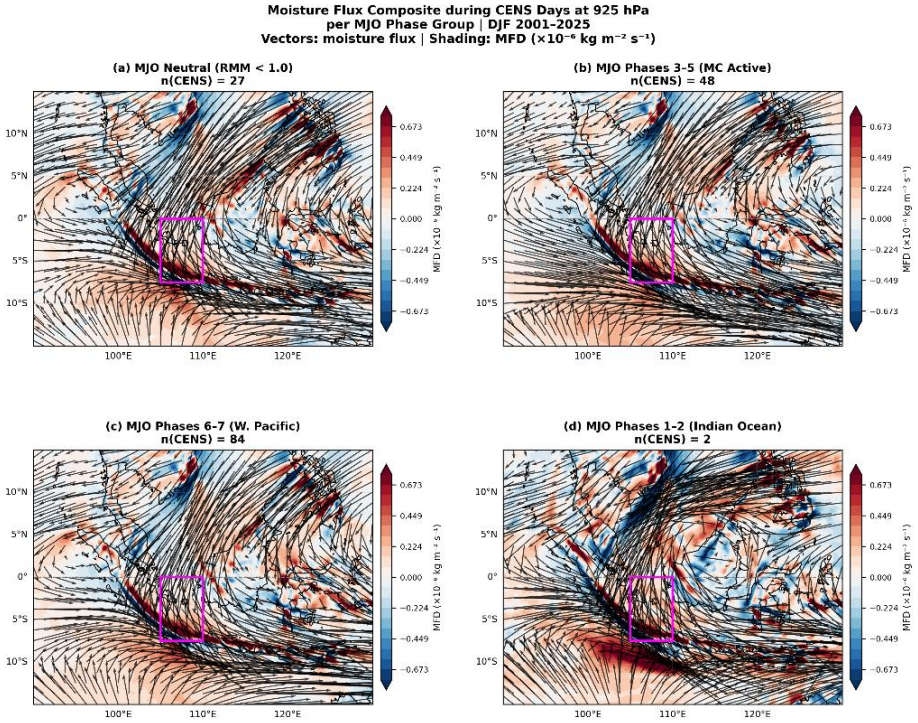


Figure 5. Moisture Flux Composite during CENS Days per MJO Phase

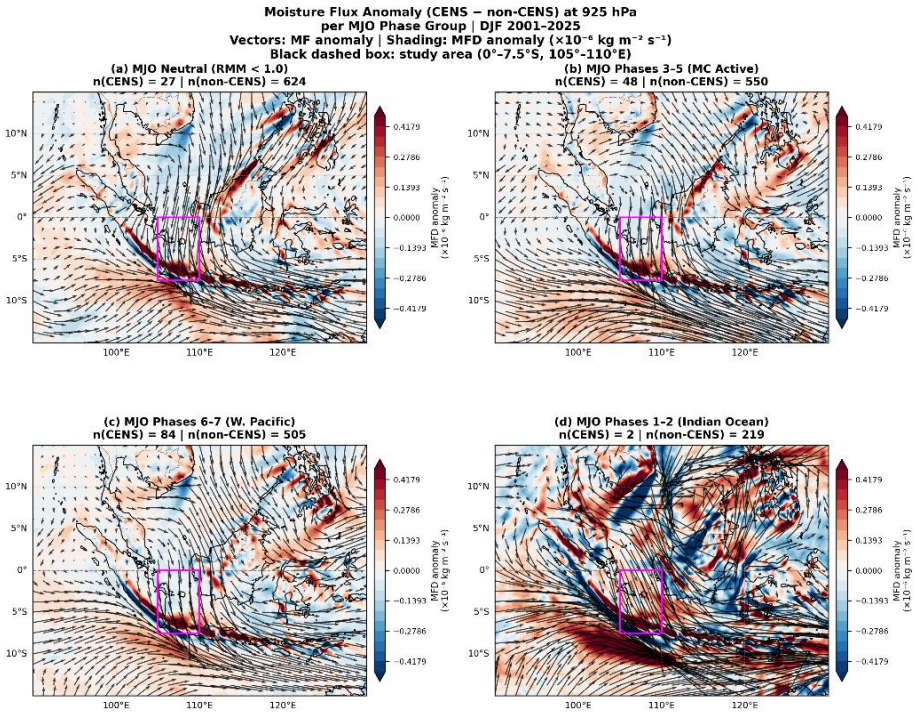


Figure 6. Moisture Flux Anomaly (CENS − nonCENS) per MJO Phase

The CENS-minus-non-CENS moisture flux anomaly composites (Figure 6) reveal that, relative to non-CENS DJF days, CENS events consistently enhance the cross-equatorial northerly moisture transport regardless of MJO phase. The most pronounced anomaly is observed during MJO phases 3–5 (Figure 6b; n(CENS) = 48, n(non-CENS) = 550), where the northerly flux anomaly vectors are strongest and the MFD anomaly over the study area is most negative —

indicating significant moisture convergence enhancement relative to non-CENS conditions. This result provides direct dynamical evidence that the rainfall intensification during CENS under MJO phases 3–5 is driven by enhanced boundary-layer moisture convergence rather than simply by stronger wind speeds alone. During MJO phases 6–7 (Figure 6c; n(CENS) = 84, n(non-CENS) = 505), the northerly flux anomaly remains statistically robust, but the magnitude of the MFD anomaly over the study area is reduced compared to phases 3–5, consistent with the paradox identified in Section 3.2.1 — CENS events are most frequent but produce less intense rainfall during these phases. During MJO-neutral conditions (Figure 6a-anomaly; n(CENS) = 27, n(non-CENS) = 624), the anomaly pattern indicates that even without active MJO support, CENS events generate a detectable moisture convergence anomaly over the study area, suggesting that cold surge-driven northerly flow alone is sufficient to enhance low-level moisture convergence over the southwestern MC, albeit less efficiently than when supported by active MJO convection.

Taken together, the lagged correlation and moisture flux anomaly analyses provide complementary evidence for the physical mechanism linking MJO to CENS: the MJO modulates the strength and organization of cross-equatorial moisture transport during CENS, with phases 3–5 producing the most efficient moisture convergence over the study area despite accounting for fewer CENS event-days than phases 6–7.

3.4. Spatial Rainfall Distribution during CENS per MJO Phase

The spatial distribution of composite daily precipitation during CENS events, stratified by dominant MJO phase, is presented in Figure 7. Only phases 4–7 are shown, as these account for the overwhelming majority of CENS event-days (171 of 276 total, ~62%) and represent the phases during which meaningful rainfall composites can be constructed. No CENS events were recorded during MJO phases 2–3, and the sample sizes for phases 1 and 8 were insufficient for reliable composite analysis.

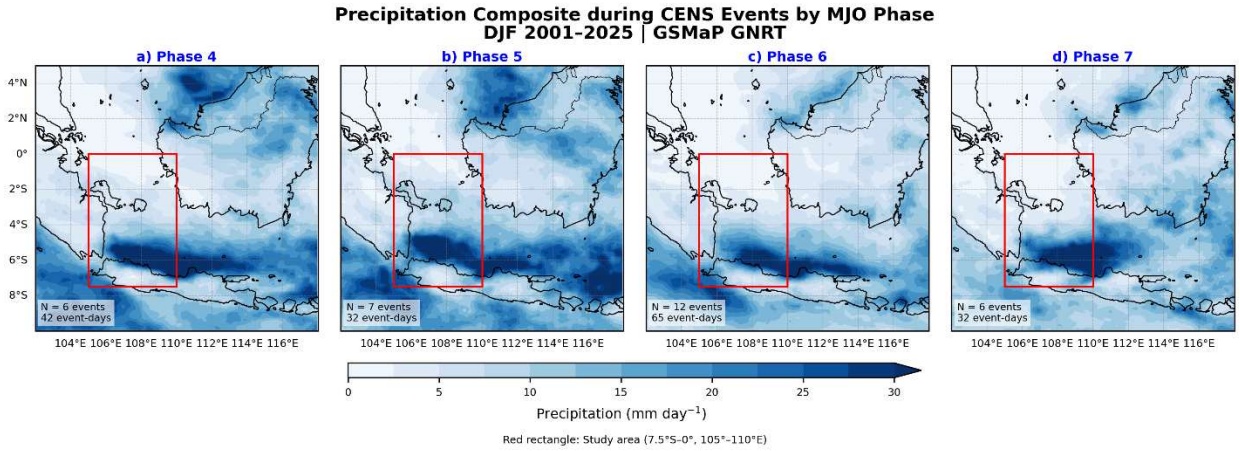


Figure 7. Composite Rainfall per MJO Phase

During MJO phase 4 — when the MJO convective envelope is transitioning from the Indian Ocean into the western Maritime Continent — composite daily precipitation over the study area is the highest among all phase groups, with widespread rainfall exceeding 20–30 mm day^{-1} across both the oceanic northern sector and the land areas of western Java and Lampung (Figure 7a; N = 6 events, 42 event-days). The enhanced rainfall extends broadly across the Karimata Strait and the western Java Sea, reflecting the combined effect of northerly moisture transport driven by CENS and the direct convective forcing of the MJO positioned over the MC. Pronounced orographic enhancement is evident along the southern mountain ranges of Java (approximately 6°–8°S), where rainfall maxima are consistently observed across all phase groups.

As the MJO propagates eastward into phase 5, the spatial pattern shifts toward greater concentration of heavy rainfall over coastal and land areas (Figure 7b; N = 7 events, 32 event-days), with the oceanic northern sector showing a relative decrease compared to phase 4. This transition is consistent with the progressive displacement of the MJO convective center eastward across the MC, which reduces the direct oceanic convective forcing while the northerly CENS flow continues to channel moisture toward the Java coastline. The coastal-land rainfall gradient becomes more pronounced in phase 5, foreshadowing the area-dependent diurnal response examined in Section 3.5.

During MJO phases 6 and 7, when MJO convection has shifted to the Western Pacific, a striking contrast emerges between event frequency and rainfall intensity — the central paradox identified in this study. Phase 6 records the highest number of CENS events (12 events) and event-days (65 event-days) of any phase group (Figure 7c), yet the composite daily rainfall within the study area is markedly weaker than during phases 4–5, with values predominantly

below 10–15 mm day⁻¹ over most of the area. Phase 7 shows the weakest rainfall of all groups (Figure 7d; N = 6 events, 32 event-days), with the study area characterized by near-climatological rainfall values despite the presence of active CENS-level northerly flow. This divergence between CENS frequency and rainfall intensity confirms that while the large-scale circulation pattern during phases 6–7 is conducive to sustaining northerly flow across the equator, the reduced MJO convective forcing over the MC substantially limits the moisture convergence and convective development associated with each CENS episode — a finding supported by the moisture flux anomaly analysis in Section 3.3.2, which showed weaker MFD anomalies over the study area during phases 6–7 compared to phases 3–5. Across all phase groups, rainfall is predominantly concentrated south of the equator within the study area, reflecting the climatological position of the ITCZ during boreal winter and the role of CENS in reinforcing convergence along the northern coast of Java. The red rectangle (0°–7.5°S, 105°–110°E) consistently captures the core region of CENS-driven rainfall enhancement, with the most intense and spatially coherent signals observed during MJO phases 4–5.

3.5. Spatially Contrasting Diurnal Rainfall Responses to CENS

Composite hourly rainfall during CENS days and non-CENS DJF days across the three study areas is presented in Figure 8. The results reveal a striking and systematic spatial contrast in the CENS-induced diurnal signal — from strong suppression over the open ocean to pronounced nocturnal enhancement over land — that constitutes the primary novel finding of this study.

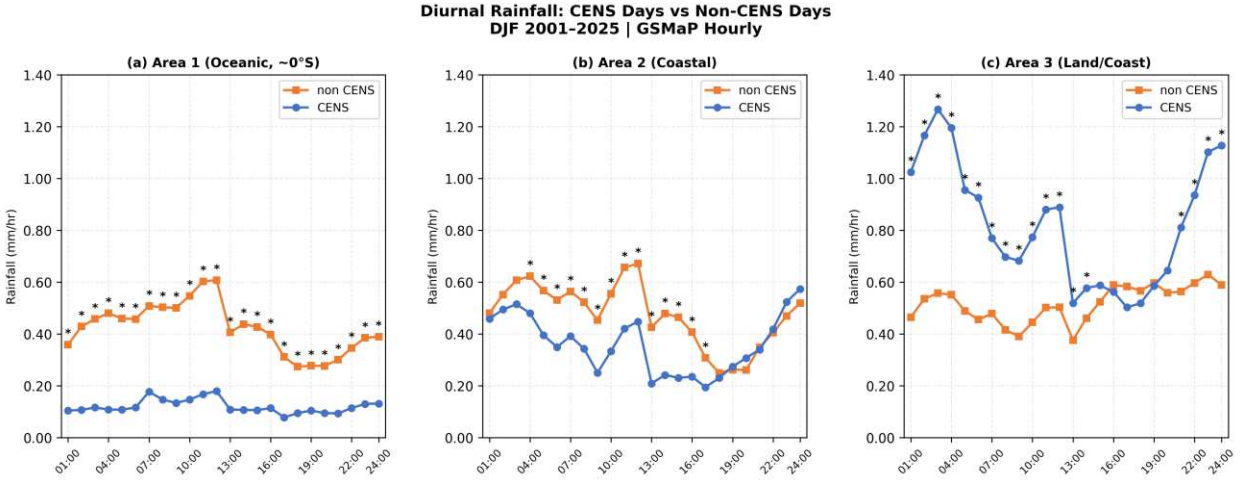


Figure 8. Diurnal Rainfall for CENS days vs non CENS Days in 3 Areas

Area 1 — Oceanic (~0°S, Karimata Strait): Over the oceanic area (Figure 8a), CENS days are characterized by near-complete suppression of hourly rainfall throughout the entire diurnal cycle, with CENS-day rainfall remaining between 0.10 and 0.19 mm hr⁻¹ — approximately 70–80% below non-CENS values at nearly all hours. Non-CENS days exhibit a well-defined diurnal cycle with a pronounced late-morning peak near 10:00–12:00 LT (~0.60 mm hr⁻¹), consistent with the thermally driven oceanic convection characteristic of the equatorial MC during boreal winter (Mori et al. 2004; Hadi et al. 2002). During CENS, this diurnal cycle is almost entirely eliminated — replaced by a weak, temporally invariant rainfall signal that shows no meaningful peak at any hour. Statistically significant differences between CENS and non-CENS conditions are detected across the majority of the 24-hour cycle (asterisks, $p < 0.05$), confirming that the suppression is robust and not attributable to sampling variability. This pervasive suppression is consistent with the advection of dry continental air by the enhanced northerly flow, which increases low-level wind shear, reduces surface moisture flux convergence, and inhibits the development of deep convection over the open ocean near the equator.

Area 2 — Coastal Transition Zone: The coastal area (Figure 8b) displays an intermediate response. Non-CENS days exhibit a bimodal diurnal pattern with peaks near 04:00 LT (~0.60 mm hr⁻¹) and 11:00 LT (~0.67 mm hr⁻¹), reflecting the interplay between nocturnal offshore flow and daytime sea-breeze-driven convection characteristic of the coastal MC environment (Mori et al. 2018; Lestari et al. 2022). During CENS, rainfall is generally suppressed relative to non-CENS conditions across most hours, though the magnitude of suppression (~20–40%) is considerably smaller than in Area 1, and the CENS-day diurnal signal retains some structural similarity to the non-CENS pattern. Statistically significant differences are confined to selected hours, indicating that the CENS influence in this transitional zone is real but inconsistent across the full diurnal cycle. This attenuated response reflects the competing influences of CENS-driven oceanic suppression and land-surface forcing in a zone where neither mechanism dominates.

Area 3 — Land/Coast (Western Java and Lampung): The land area (Figure 8c) presents a response that is diametrically opposite to Area 1 — one of the most striking findings of this study. During CENS days, hourly rainfall is dramatically enhanced relative to non-CENS conditions across nearly all hours, with CENS-day values ranging from approximately 0.60 to 1.27 mm hr^{-1} compared to the relatively flat non-CENS climatology of 0.40–0.60 mm hr^{-1}. The enhancement is most pronounced during the nocturnal and early-morning hours, with a primary peak near 02:00–04:00 LT (~1.20–1.27 mm hr^{-1}) and a secondary peak near 22:00–24:00 LT (~0.95–1.13 mm hr^{-1}). Statistical significance is confirmed across the majority of hours (asterisks, $p < 0.05$). The non-CENS diurnal cycle in Area 3 is comparatively subdued and lacks the strong nocturnal amplification characteristic of CENS conditions, confirming that the nocturnal rainfall intensification over western Java is a CENS-specific signal rather than a background climatological feature.

The pronounced nocturnal peak during CENS in Area 3 reflects several reinforcing mechanisms. The enhanced northerly flow transports cool, moisture-laden air from the South China Sea southward toward the Java coastline, where it converges with the thermally driven upslope flow along the northern flanks of the Java mountain ranges. This orographic lifting, combined with the stabilizing influence of the nocturnal land breeze over the ocean, promotes the development of organized mesoscale convective systems that preferentially develop and intensify during the late-night and early-morning hours — consistent with the nocturnal convection mechanisms documented by Mori et al. (2018) and Yulihastin et al. (2020) for the Jakarta metropolitan area. The result is a systematic CENS-driven redistribution of rainfall from the ocean to the land surface, with potentially severe implications for flood risk in the densely populated lowlands of western Java, where nocturnal rainfall is the dominant driver of flash flooding events (Wu et al. 2007; Lubis et al. 2022; Lubis et al. 2025).

Synthesis: The three-area comparison reveals that CENS does not simply amplify the existing boreal winter diurnal cycle uniformly, but fundamentally reorganizes the spatial distribution of convective rainfall across the ocean-to-land gradient. The suppression–enhancement contrast between Area 1 and Area 3 exceeds a factor of 5–7 in peak hourly rainfall during CENS versus non-CENS conditions, and is statistically significant at the 5% level across the majority of the 24-hour cycle in both areas. This area-dependent reorganization — driven by the differential response of oceanic and land-based convection to enhanced low-level northerly flow — constitutes the primary novel contribution of this study and has not been previously documented through a systematic CENS versus non-CENS day comparison across the ocean-coast-land gradient of the southwestern Maritime Continent.

4. DISCUSSION

4.1. MJO Modulation of CENS: Frequency, Intensity, and Temporal Sequencing

The results of this study reveal a fundamental paradox in the MJO–CENS relationship that has not been explicitly documented in prior work: CENS events occur most frequently when MJO convection is positioned over the Western Pacific (phases 6–7), yet the most intense rainfall within the study area is observed when MJO convection is active over the Maritime Continent itself (phases 4–5). This distinction has important implications for both the physical understanding of CENS dynamics and for operational forecasting. The dominance of phases 6–7 in CENS event-day frequency (Table 6) reflects the well-established role of the MJO in modulating the large-scale pressure gradient between the Asian continent and the equatorial MC. As the MJO convective envelope propagates eastward into the Western Pacific, the suppressed convection phase over the MC strengthens the anticyclonic flow over the South China Sea, enhancing the northerly cross-equatorial pressure gradient and favoring the development of sustained northerly low-level flow (Lubis et al. 2023). This mechanism operates even as the direct convective forcing of the MJO over the MC wanes, explaining why CENS events remain frequent during phases 6–7 despite reduced local convective instability. In contrast, the rainfall intensity maximum during phases 4–5 reflects the combined effect of two reinforcing mechanisms. First, the direct MJO convective forcing over the MC during these phases destabilizes the atmosphere and increases precipitable water over the study area. Second, the northerly moisture transport driven by CENS simultaneously enhances low-level moisture convergence along the northern coast of Java. The moisture flux anomaly composites (Figure 6) provide direct dynamical evidence for this synergy: during MJO phases 3–5, the CENS-minus-non-CENS MFD anomaly over the study area is most strongly negative — indicating the greatest moisture convergence enhancement — consistent with the rainfall maxima observed in the composite precipitation analysis (Figure 5). During phases 6–7, the MFD anomaly weakens despite persistent northerly flow, confirming that the rainfall response is governed not by wind speed alone but by the efficiency of moisture convergence, which declines as MJO convective forcing withdraws from the MC. This finding extends the understanding presented by Moteki (2024), who identified CENS intensification under active MJO conditions but did not separate the frequency and intensity responses across individual phases, and is consistent with the projected amplification of CENS-induced precipitation described by Lubis et al. (2025), who attributed enhanced future rainfall to increased moistening efficiency under warming rather than changes in CENS frequency or intensity per se.

The lagged correlation analysis further advances the physical understanding of this relationship by providing temporal evidence that MJO activity systematically precedes CENS intensification. The progressive strengthening of the negative correlation from lag −6 to lag −1 days (Figure 4a) indicates that enhanced MJO amplitude — reflecting stronger and more organized intraseasonal convection — precedes the intensification of northerly flow over the study area by approximately one to six days. This lead time is physically consistent with the eastward propagation speed of the MJO (~5–8 m s^{-1}) and the downstream adjustment of the large-scale circulation over the MC, which operates on the timescale of a few days through Kelvin wave and boundary layer responses (Wheeler and Hendon 2004; Lubis et al. 2023). The strengthening of the lagged correlation when restricted to MC-active MJO phases (3–7; Figure 4b, peak $r = -0.074$, $p < 0.001$) confirms that this temporal sequencing is physically meaningful rather than a statistical artifact of the phase-blind RMM amplitude metric — directly addressing the concern raised by previous reviewers that such correlations may conflate the effects of MJO amplitude across dynamically distinct phases. The quasi-simultaneous peak (lag ≈ 0 to +2 days) is consistent with the rapid boundary-layer adjustment to MJO convective heating documented for cross-equatorial flow dynamics over the southwestern MC (Lubis et al. 2023).

4.2. ENSO and IOD as Co-modulators of CENS

The elevated CENS frequency during La Niña (28 events, 53.8%) relative to neutral (19 events, 36.5%) and El Niño (5 events, 9.6%) conditions is consistent with the well-documented strengthening of the Asian winter monsoon circulation during La Niña years, which enhances the meridional pressure gradient driving northerly low-level flow across the equator (Moteki 2024; Hadi et al. 2025). However, the mechanism through which La Niña modulates CENS is not purely independent — the chi-square analysis reveals that La Niña significantly alters the MJO phase distribution during DJF ($\chi^2 = 33.779$, df = 14, $p = 0.0022$), with La Niña seasons exhibiting the highest number of active MJO days (643 days) and a greater proportion of MJO activity in phases 6–7 compared to neutral and El Niño conditions. This result implies that La Niña enhances CENS frequency through two partially overlapping pathways: directly, by strengthening the background northerly monsoon flow, and indirectly, by prolonging the duration of active MJO conditions — particularly in the phases most conducive to CENS development. This dual mechanism is consistent with the theoretical framework proposed by Lubis et al. (2023), who demonstrated that CENS events and the MJO interact through a positive feedback — cross-equatorial surges strengthen the southward detour of the MJO over the MC, while active MJO phases in turn favor CENS development — a feedback that would be amplified under the stronger monsoon background flow characteristic of La Niña years. The persistence of CENS events during El Niño (5 events, 9.6%), despite the typically reduced northerly monsoon flow associated with warm ENSO conditions, demonstrates that CENS is not fully suppressed even during El Niño, consistent with the findings of Hadi et al. (2025) for a longer observational record. The occurrence of El Niño-period CENS events predominantly in combination with cold surges (1 MJO+CS event and 3 noMJO+CS events out of 5 El Niño events; Table 3) suggests that during El Niño, extratropical cold surge forcing plays a proportionally larger role in CENS initiation — compensating for the weaker background monsoon circulation.

Regarding the IOD, the analysis reveals that the large majority of CENS events (69.2%) occurred during neutral IOD conditions, with IOD-negative events accounting for 25.0% and IOD-positive for only 5.8% (Figure 3). While the slightly elevated frequency during IOD-negative compared to IOD-positive conditions is physically plausible — IOD-negative years are associated with anomalous SST warming in the eastern tropical Indian Ocean that may enhance cross-equatorial pressure gradients — the small sample sizes preclude robust statistical attribution. The IOD is therefore most appropriately characterized as a secondary co-modulator of CENS, operating through its influence on the background Indian Ocean SST gradient and associated changes in monsoon circulation, rather than as an independent driver. Future studies employing longer observational records or large-ensemble model simulations will be needed to definitively characterize the IOD–CENS relationship, particularly given the documented co-variability between ENSO and IOD states on interannual timescales (Saji et al. 1999).

4.3. Physical Mechanisms of the Spatially Contrasting Diurnal Rainfall Response

The spatially contrasting diurnal responses to CENS across the three study sub-areas constitute the primary novel finding of this study and warrant detailed mechanistic interpretation. The suppression–enhancement contrast — from near-complete rainfall suppression in the oceanic Area 1 to dramatic nocturnal amplification in the land Area 3 — exceeds a factor of 5–7 in peak hourly rainfall between CENS and non-CENS conditions, and is statistically significant at the 5% level across the majority of the 24-hour cycle in both extreme areas. Over the oceanic area (Area 1), the pervasive rainfall suppression during CENS reflects the disruption of the thermally driven oceanic convective cycle by the enhanced northerly low-level flow. Under non-CENS conditions, the diurnal rainfall cycle over the equatorial MC is governed by the interplay between solar heating, boundary-layer moisture accumulation, and sea surface fluxes, producing a characteristic late-morning convective peak around 10:00–12:00 LT (Mori et al. 2004; Hadi et al. 2002). The intrusion of strong northerly flow during CENS increases low-level wind shear, reduces the residence time of

boundary-layer air over the warm sea surface, and suppresses the low-level moisture convergence necessary to sustain deep convection. Additionally, the cool and relatively dry continental air advected southward from the Asian continent during CENS reduces the equivalent potential temperature of the boundary layer, further inhibiting convective instability over the open ocean. The absence of any meaningful diurnal structure in the CENS-day rainfall over Area 1 — in contrast to the well-defined non-CENS peak — indicates that the thermodynamic suppression by the northerly flow completely overrides the local diurnal forcing mechanisms that normally drive oceanic convection in this region. The coastal Area 2 exhibits an intermediate response that reflects the competing influences of oceanic suppression and land-surface forcing in a transition zone where neither mechanism dominates completely. The partial retention of the non-CENS diurnal structure during CENS conditions, combined with statistically significant differences at selected hours, suggests that the coastal geometry of western Java — where the ITCZ convergence zone intersects with the land-sea boundary — partially shields the coastal precipitation regime from the full suppressive influence of the offshore northerly flow. This transitional behavior is consistent with the longitudinal variation of CENS impacts across Java documented by Maulana et al. (2023), who showed that the CENS influence weakens progressively from the western to the eastern end of the island. Over the land area (Area 3), the dramatic nocturnal rainfall enhancement during CENS — with a primary peak at 02:00–04:00 LT and a secondary peak near 22:00–24:00 LT, both approximately double the non-CENS values — results from the constructive superposition of three distinct forcing mechanisms. First, the enhanced northerly moisture flux during CENS systematically increases the low-level moisture supply to the northern slopes of the Java mountain ranges, providing additional precipitable water for convective development compared to non-CENS conditions. Second, the orographic lifting of this enhanced moisture-laden northerly flow along the northern flanks of the Bogor–Puncak–Cianjur mountain complex (elevation >2,000 m) intensifies upward motion and promotes the organization of mesoscale convective systems, as documented by Satiadi et al. (2023) for the latitudinal dependence of CENS-driven rainfall across West Java. Third, during the nocturnal hours, the land breeze from the Java interior reinforces the convergence of the northerly CENS flow at the coast, creating a narrow convergence zone that further intensifies precipitation, consistent with the nocturnal coastal convergence mechanism described by Mori et al. (2018) for the Jakarta metropolitan region. The secondary late-evening peak (22:00–24:00 LT) likely reflects the offshore propagation of convective systems initiated earlier over the mountains, consistent with the westward-propagating mesoscale convective systems documented over western Java during boreal winter (Yulihastin et al. 2020).

The resulting redistribution of rainfall from ocean to land during CENS — from suppression over the Karimata Strait to enhancement over the northern Java lowlands — has profound implications for the interpretation of CENS as a rainfall driver. Previous studies have characterized CENS primarily as a mechanism for enhancing rainfall along the northern Java coast in general (Wu et al. 2007; Hattori et al. 2011; Lubis et al. 2022), but the present analysis demonstrates that this enhancement is highly spatially selective, concentrated in the nocturnal hours, and accompanied by an equally significant suppression over the adjacent ocean. This spatial selectivity implies that the net area-integrated rainfall effect of CENS over the southwestern MC may be smaller than suggested by coastal station observations alone, and that the oceanic rainfall deficit during CENS may partially offset the land-surface enhancement when considering the regional water budget.

4.4. Implications for Flood Risk and Early Warning

The nocturnal rainfall amplification over the land area during CENS — reaching peak hourly intensities of 1.20–1.27 mm hr^{-1} around 02:00–04:00 LT — has direct and severe implications for flood risk management in western Java. Jakarta, situated on the northern coastal plain of western Java at elevations below 10 m above sea level, is acutely vulnerable to rapid surface runoff generated by intense nocturnal rainfall over the Bogor–Puncak highlands upstream, which can reach the Jakarta metropolitan area within hours through the Ciliwung and Cisadane river systems (Wu et al. 2007; Budiyono et al. 2015; Lubis et al. 2022). The systematic amplification of nocturnal rainfall by a factor of approximately 2 during CENS conditions, relative to non-CENS DJF nights, implies that CENS-active periods represent a substantially elevated flood risk window that is not fully captured by daily rainfall monitoring systems or current operational early warning frameworks.

The lagged correlation results offer a practical pathway toward improved early warning. The finding that MJO amplitude over the MC systematically precedes CENS intensification by 3–6 days suggests that real-time monitoring of the RMM index — particularly the onset of active MJO conditions in phases 3–7 — could provide a 3–6 day advance signal for heightened CENS probability and associated nocturnal flood risk over western Java. When combined with La Niña monitoring through the ONI, which is available in near-real-time from NOAA, this framework provides a multi-scale early warning capability spanning seasonal (ENSO), intraseasonal (MJO), and synoptic (CENS) timescales — consistent with the integrated monitoring approach advocated for Southeast Asian hydrometeorological hazards (Lubis et al. 2025). Furthermore, the projected intensification of CENS-associated extreme precipitation under

future warming scenarios described by Lubis et al. (2025) — attributed to enhanced atmospheric moistening efficiency rather than changes in CENS dynamics per se — implies that the nocturnal rainfall amplification documented here is likely to intensify in a warmer climate, further elevating flood risk in western Java's urban areas and underscoring the urgency of integrating CENS dynamics into long-term urban drainage planning and disaster risk reduction frameworks.

4.5. Limitations and Future Directions

Several limitations of this study merit acknowledgment. First, the 25-year study period (DJF 2001–2025), while substantially longer than many previous CENS investigations, yields a total of 52 events — a sample size that is sufficient for composite analyses but results in small sub-group samples when events are stratified simultaneously by MJO phase, ENSO state, CS co-occurrence, and IOD state (Table 3). Several sub-categories, particularly El Niño conditions (5 events) and IOD-positive conditions (3 events), are too small for robust statistical inference, and conclusions drawn from these subsets should be interpreted with appropriate caution.

Second, the lagged correlation analysis, while providing temporal evidence for MJO–CENS sequencing, does not constitute formal causal attribution in the dynamical systems sense. The moisture flux anomaly composites provide complementary spatial dynamical evidence, but a formal attribution would require Lagrangian trajectory analysis or numerical model sensitivity experiments isolating the MJO forcing. Third, the diurnal rainfall analysis employs GSMaP satellite precipitation, which, despite gauge adjustment, may underestimate orographic rainfall over the Java highlands and overestimate rainfall over the open ocean during periods of strong low-level wind shear — precisely the conditions that characterize CENS events. Ground-based radar or rain gauge networks over Java would provide valuable validation of the diurnal signals documented here. Fourth, the role of the IOD as a secondary co-modulator remains statistically inconclusive given the small sample of IOD-positive events, and the potential influence of mesoscale factors — including the Borneo Vortex, equatorial waves, and local sea-surface temperature anomalies in the Java Sea — on CENS variability has not been formally assessed in this study.

Future work should extend the analysis to longer reanalysis records (e.g., ERA5 back to 1940) to increase sample sizes and improve the statistical robustness of the ENSO- and IOD-stratified composites. Numerical model experiments using an atmospheric general circulation model with prescribed MJO forcing could provide formal causal evidence for the lagged MJO–CENS relationship identified here. Additionally, the potential amplification of the nocturnal CENS-driven rainfall enhancement under future climate change — as projected by Lubis et al. (2025) — warrants investigation using the dynamical framework developed in this study, particularly in the context of urban flood risk assessment for the Jakarta metropolitan area.

5. CONCLUSIONS

This study investigated the characteristics and large-scale modulation of cross-equatorial northerly surge (CENS) events over the southwestern Maritime Continent (0°–7.5°S, 105°E–110°E) during boreal winter (DJF) over a 25-year period (2001–2025), with particular emphasis on three aspects that have not been systematically addressed in prior literature. A total of 52 CENS events (2.08 events per year) were identified following the Hattori et al. (2011) domain criteria using ERA5 925 hPa reanalysis, with event durations predominantly in the 3–7 day range (87%). CENS occurrence was most frequent during La Niña (53.8%) and in association with active MJO conditions (76.9%), with cold surges co-occurring in 73.1% of events. A statistically significant association between ENSO state and MJO phase distribution was confirmed ($\chi^2 = 33.779$, $p = 0.0022$), indicating that La Niña enhances CENS frequency partly by prolonging active MJO conditions — particularly in phases 6–7 — rather than solely through direct strengthening of the monsoon flow. The IOD was identified as a secondary co-modulator, with most CENS events (69.2%) occurring during neutral IOD conditions.

A key finding is the paradox between MJO phase frequency and rainfall intensity: while CENS event-days are most frequent during MJO phases 6–7, the most intense rainfall over the study area occurs during phases 4–5. Moisture flux anomaly composites demonstrate that this contrast is dynamically driven by phase-dependent differences in boundary-layer moisture convergence efficiency — strongest during phases 3–5 when MJO convection directly overlies the Maritime Continent. Lagged correlation analysis, filtered for MC-active MJO phases (3–7), confirms that enhanced MJO activity temporally precedes CENS intensification by 3–6 days (peak $r = -0.074$, $p < 0.001$), providing evidence for a systematic temporal sequencing beyond simple co-occurrence. The primary novel contribution of this study is the systematic documentation of spatially contrasting diurnal rainfall responses to CENS across the ocean-to-land gradient. CENS suppresses hourly rainfall over the oceanic area by 70–80% throughout the diurnal cycle, while simultaneously enhancing nocturnal rainfall over the land area by a factor of approximately two, with statistically significant peaks at 02:00–04:00 LT and 22:00–24:00 LT. This area-dependent redistribution — from oceanic suppression to nocturnal land enhancement — reflects the differential response of oceanic and orographically forced convection to enhanced northerly flow, and has not been previously documented through a systematic CENS versus

non-CENS day comparison across the full ocean-coast-land gradient. The nocturnal rainfall amplification over western Java during CENS carries direct implications for flash flood risk in the Jakarta metropolitan area and supports the integration of MJO and ENSO monitoring into multi-scale early warning frameworks for hydrometeorological hazards in the southwestern Maritime Continent.

Acknowledgements. The authors would like to acknowledge the use of data in this study. The RMM1 and RMM2 index data were obtained from the Australian Bureau of Meteorology (http://www.bom.gov.au/climate/mjo/graphics/rmm.74toRealtime.txt). The Global Rainfall Map (GSMaP) by the Japan Aerospace Exploration Agency (JAXA) Global Rainfall Watch' was produced and distributed by the Earth Observation Research Center, Japan Aerospace Exploration Agency. Meteorological Satellites of MTSAT and Himawari-8 data are provided by the Japan Meteorological Agency (JMA). ERA5 reanalysis data from Hersbach et al. (2023) was downloaded from the Copernicus Climate Change Service (C3S). The results presented contain modified Copernicus Climate Change Service information (2020). Neither the European Commission nor ECMWF is responsible for any use of the Copernicus information or data contained herein.
Competing Interest : The authors declare that they have no conflicts of interest.

References.

Aldrian, E., Susanto, R.D (2003) Identification of three dominant rainfall regions within Indonesia and their relationship to sea surface temperature. International Journal of Climatology 23(12), 1435–1452. https://doi.org/10.1002/joc.950

Barnston, A.G., Chelliah, M., Goldenberg, S.B (1997) Documentation of a highly ENSO-related SST region in the equatorial Pacific. Atmosphere-Ocean 35, 367–383. https://doi.org/10.1080/07055900.1997.9649597

Budiyono, Y., Aerts, J., Brinkman, J.J., Marfai, M.A., Ward, P (2015) Flood risk assessment for delta mega-cities: a case study of Jakarta. Natural Hazards 75, 389–413. https://doi.org/10.1007/s11069-014-1327-9

Chang, C.P., Wang, Z., McBride, J., Liu, C (2005) Annual cycle of Southeast Asia - Maritime Continent rainfall and the asymmetric monsoon transition. Journal of Climate 18, 287–301. https://doi.org/10.1175/JCLI-3257.1

Crook, J., Hardy, S., Methven, J., Schwendike, J., Yik, D.J., Yang, G.Y (2024) The structure of Borneo vortices and their relationship with cold surges, the Madden-Julian oscillation and equatorial waves. Quarterly Journal of the Royal Meteorological Society 151(766), 1–25. https://doi.org/10.1002/qj.4905

Hadi, T.W., Horinouchi, T., Tsuda, T., Hashiguchi, H., Fukao, S (2002) Sea-breeze circulation over Jakarta, Indonesia: A climatology based on boundary layer radar observations. Monthly Weather Review 130, 2153–2166. https://doi.org/10.1175/1520-0493(2002)130<2153:SBCOJI>2.0.CO;2

Hadi, T.W., Abdillah, M.R., Purwadani, N.N., Suwarman, R., Trilaksono, N.J., Fajary, F.R., Maulana, M.T., Wijaya, D.D (2025) Cross-equatorial northerly surges associated with extratropical cold surges and tropical variability over the Maritime Continent. Journal of Climate 38, 2783–2798. https://doi.org/10.1175/JCLI-D-24-0132.1

Hattori, M., Mori, S., Matsumoto, J (2011) The cross-equatorial northerly surge over the Maritime Continent and its relationship to precipitation patterns. Journal of the Meteorological Society of Japan 89A, 27–47. https://doi.org/10.2151/jmsj.2011-A02

Heo, J.W., Ho, C.H., Park, T.W., Choi, W., Jeong, J.H., Kim, J (2018) Changes in cold surge occurrence over East Asia in the future: Role of thermal structure. Atmosphere 9, 1–16. https://doi.org/10.3390/atmos9060222

Hersbach, H., Bell, B., Berrisford, P., Biavati, G., Horanyi, A., Munoz Sabater, J., Nicolas, J., Peubey, C., Radu, R., Rozum, I., Schepers, D., Simmons, A., Soci, C., Dee, D., Thepaut, J.N (2023) ERA5 hourly data on pressure levels from 1940 to present. Copernicus Climate Change Service (C3S) Climate Data Store (CDS). https://doi.org/10.24381/cds.bd0915c6. Accessed 18 February 2025

Hersbach, H., Bell, B., Berrisford, P., Hirahara, S., Horanyi, A., Munoz-Sabater, J., Nicolas, J., Peubey, C., Radu, R., Schepers, D., Villaume, S., Thepaut, J.N (2020) The ERA5 global reanalysis. Quarterly Journal of the Royal Meteorological Society 146, 1999–2049. https://doi.org/10.1002/qj.3803

Kubota, T., Aonashi, K., Ushio, T., Shige, S., Takayabu, Y.N., Kachi, M., Arai, Y., Tashima, T., Masaki, T., Kawamoto, N., Mega, T (2020) Global Satellite Mapping of Precipitation (GSMaP) products in the GPM era. In Satellite precipitation measurement: Volume 1, pp. 355–373. Cham: Springer International Publishing. https://doi.org/10.1007/978-3-030-24568-9_20

Lestari, S., Protat, A., Louf, V., King, A., Vincent, C., and Mori, S (2022) Subdaily rain-rate properties in western Java analyzed using C-band Doppler radar. Journal of Applied Meteorology and Climatology, 61(9), 1199–1219. https://doi.org/10.1175/JAMC-D-21-0041.1

Liu, P., Zhang, Q., Zhang, C., Zhu, Y., Khairoutdinov, M., Kim, H.M., Schumacher, C., Zhang, M (2016) A revised real-time multivariate MJO index. Monthly Weather Review 144, 627–642. https://doi.org/10.1175/MWR-D-15-0237.1

Lubis, S.W., Chang, C.C., Hagos, S., Zhao, M., Chen, Z., Balaguru, K., Leung, L.R (2025) Projected changes in cross-equatorial northerly surges and their hydrological impacts in the near future. npj Clim Atmos Sci 8, 375. https://doi.org/10.1038/s41612-025-01239-x

Lubis, S.W., Hagos, S., Hermawan, E., Respati, M.R., Ridho, A., Risyanto, Paski, J.A., Muhammad, F.R., Siswanto, Ratri, D.N., Setiawan, S (2022) Record-breaking precipitation in Indonesia's capital of Jakarta in early January 2020 linked to the northerly surge, equatorial waves, and MJO. Geophysical Research Letters 49(22), e2022GL101513. https://doi.org/10.1029/2022GL101513

Lubis, S.W., Hagos, S., Chang, C., Balaguru, K., Leung, L.R (2023) Cross-equatorial surges boost MJO's southward detour over the Maritime Continent. Geophysical Research Letters 50, 1–11. https://doi.org/10.1029/2023GL104770

Maulana, M.T., Yamazaki, T., Iwasaki, T., Abdillah, M.R (2023) Regional variation of the influence of cross-equatorial northerly surge towards diurnal cycle of rainfall over Java Island. Geoscience Letters 10, 40. https://doi.org/10.1186/s40562-023-00293-8

Mori, S., Hamada, J.I., Hattori, M., Wu, P.M., Katsumata, M., Endo, N., Ichiyanagi, K., Hashiguchi, H., Arbain, A.A., Sulistyowati, R., Lestari, S., Syamsudin, F., Manik, T., Yamanaka, M.D (2018) Meridional march of diurnal rainfall over Jakarta, Indonesia, observed with a C-band Doppler radar: an overview of the HARIMAU2010 campaign. Progress in Earth and Planetary Science 5, 47. https://doi.org/10.1186/s40645-018-0202-9

Mori, S., Jun-Ichi, H., Tauhid, Y.I., Yamanaka, M.D., Okamoto, N., Murata, F., Sakurai, N., Hashiguchi, H., Sribimawati, T (2004) Diurnal land-sea rainfall peak migration over Sumatera Island, Indonesian Maritime Continent, observed by TRMM satellite and intensive rawinsonde soundings. Monthly Weather Review 132, 2021–2039. https://doi.org/10.1175/1520-0493(2004)132<2021:DLRPMO>2.0.CO;2

Moteki, Q (2024) Vertical structure and occurrence patterns of the cross-equatorial northerly surge under different ENSO and MJO phases. Scientific Reports 14, 29116. https://doi.org/10.1038/s41598-024-80951-9

Peatman, S.C., Matthews, A.J., Stevens, D.P (2014) Propagation of the Madden-Julian Oscillation through the Maritime Continent and scale interaction with the diurnal cycle of precipitation. Quarterly Journal of the Royal Meteorological Society 140, 814–825. https://doi.org/10.1002/qj.2161

Rayner, N.A., Parker, D.E., Horton, E.B., Folland, C.K., Alexander, L.V., Rowell, D.P., Kent, E.C., Kaplan, A (2003) Global analyses of sea surface temperature, sea ice, and night marine air temperature since the late nineteenth century. Journal of Geophysical Research 108(D14), 4407. https://doi.org/10.1029/2002JD002670

Saji, N.H., Goswami, B.N., Vinayachandran, P.N., Yamagata, T (1999) A dipole mode in the tropical Indian Ocean. Nature 401, 360-363. https://doi.org/10.1038/43854

Satiadi, D., Purwaningsih, A., Harjupa, W., Trismidianto, Andarini, D.F., Nauval, F., Saufina, E., Harjana, T., Risyanto, Rahmatia, F., Pratama, R., Devianto, D., Yollanda, M (2023) Impacts of CENS and MJO phenomena on diurnal cycle of local convection, moisture convergence, and rainfall over land, coast, and sea areas in the western part of Java Island. Meteorology and Atmospheric Physics 135, 42. https://doi.org/10.1007/s00703-023-00979-w

Straub, K.H (2013) MJO initiation in the real-time multivariate MJO index. Journal of Climate 26, 1130–1151. https://doi.org/10.1175/JCLI-D-12-00074.1

Trenberth, K.E (1997) The definition of El Nino. Bulletin of the American Meteorological Society 78(12), 2771–2778. https://doi.org/10.1175/1520-0477(1997)078<2771:TDOENO>2.0.CO;2

Trilaksono, N.J., Otsuka, S., Yoden, S (2012) A time-lagged ensemble simulation on the modulation of precipitation over West Java in January-February 2007. Monthly Weather Review 140(2), 601–616. https://doi.org/10.1175/MWR-D-11-00094.1

Trismidianto, Andarini, D.F., Muharsyah, R., Purwaningsih, A., Risyanto, Nauval, F., Fathrio, I., Harjupa, W., Nuryanto, D.E., Harjana, T., Satiadi, D., Saufina, E., Praja, A.S (2023) Interactions among cold surge, cross-equatorial northerly surge, and Borneo Vortex in influencing extreme rainfall during Madden-Julian oscillation

over the Indonesia Maritime Continent. Meteorology and Atmospheric Physics 135, 43. https://doi.org/10.1007/s00703-023-00978-x

Wheeler, M.C., Hendon, H.H (2004) An all-season real-time multivariate MJO index: Development of an index for monitoring and prediction. Monthly Weather Review 132, 1917–1932. https://doi.org/10.1175/1520-0493(2004)132<1917:AARMMI>2.0.CO;2

Wu, P., Arbain, A.A., Mori, S., Hamada, J.I., Hattori, M., Syamsudin, F., Yamanaka, M.D (2013) The effects of an active phase of the Madden-Julian Oscillation on the extreme precipitation event over western Java Island in January 2013. Scientific Online Letters on the Atmosphere 9, 79–83. https://doi.org/10.2151/sola.2013-018

Wu, P., Hara, M., Fudeyasu, H., Yamanaka, M.D., Matsumoto, J., Syamsudin, F., Sulistyowati, R., Djajadihardja, Y.S (2007) The impact of trans-equatorial monsoon flow on the formation of repeated torrential rains over Java Island. Scientific Online Letters on the Atmosphere 3, 93–96. https://doi.org/10.2151/sola.2007-024

Xavier, P., Lim, S.Y., Ammar Bin Abdullah, M.F., Bala, M., Chenoli, S.N., Handayani, A.S., Marzin, C., Permana, D., Tangang, F., Williams, K.D., Yik, D.J (2020) Seasonal dependence of cold surges and their interaction with the Madden-Julian oscillation over Southeast Asia. Journal of Climate 33(6), 2467–2482. https://doi.org/10.1175/JCLI-D-19-0048.1

Yulihastin, E., Wahyu Hadi, T., Sari Ningsih, N., Ridho Syahputra, M (2020) Early morning peaks in the diurnal cycle of precipitation over the northern coast of West Java and possible influencing factors. Annales Geophysicae 38(1), 231–242. https://doi.org/10.5194/angeo-38-231-2020